Aminoquinolines: fluorescent sensors to DNA – A new minor groove probe

Abstract

d

1. Introduction

D

2. Materials and Methods

2.1 Chemicals and solutions

Deoxyribonucleic acid sodium salt from calf thymus (ct-DNA), ethidium bromide, Hoechst 33258, acridine orange, norfloxacin, indomethacin, vanillin, 4-hydroxycoumarin, 2-(N-morpholino)ethanesulfonic acid (MES) and 2-Amino-2-(hydroxymethyl)-1,3-propanediol (TRIS) were obtained from Sigma-Aldrich Chemical Co. (St. Louis, MO, USA). Stock solutions of DNA were prepared by dissolving approximately 1-2 mg of DNA fibers in 2 mL 50 mM Tris-HCl buffer (pH 7.0) by shaking gently and stored for 24 h at 4°C. The concentration of DNA was determined by spectrophotometry at 260 nm using an extinction coefficient of 6600 M^{-1} cm^{-1} [1]. The aminoquinolines were available in our lab from a recent project. See Pastrello *et al.* for details of synthesis and characterization [2]. The stock solutions of aminoquinolines (10 mM) and drugs were prepared in dimethyl sulfoxide. All reagents used for preparing solutions and buffers were of analytical grade. All solutions were prepared with water purified by a Milli-Q system (Millipore, Bedford, MA, USA).

2.2 General steady-steady fluorescence studies

Fluorescence spectra were obtained using a Perkin Elmer LS 55 spectrofluorimeter (Shelton, CT, USA), and measurements were performed using a 3 mL quartz cuvette with constant

magnetic stirring. The slit widths were set at 10 nm for excitation and emission wavelengths. The wavelengths were set at 495 nm for excitation and 530–600 nm for emission (aminoquinoline-DNA); 490 nm and 505 – 620 nm (acridine orange-DNA); 340 nm and 355 – 650 nm (Hoechst-DNA); 500 nm and 530–700 nm (ethidium bromide-DNA). The experimental condition, including concentrations of the fluorescent probes, DNA, buffer constituents, and pH, were varied and will be presented in the figure legends. The buffers used were 10 mM formic acid-NaOH (pH 3.0-4.0), 10 mM citric acid-NaOH (pH 5.0-6.0), 10 mM MES-HCl (pH 5.0-7.0) and 10 mM TRIS-HCl (pH 7.0-9.0).

2.3 Fluorescence Anisotropy studies

The fluorescence anisotropy of the aminoquinolines was measured in the absence or presence of nucleic acid. The experimental conditions were: aminoquinolines (5.0 µM), DNA (50 µM) in 10 mM TRIS-HCl, pH 7.0, 25°C. The excitation was set at 500 nm and the emission at 590 nm. The anisotropy of free aminoquinoline was measured in 1,2-dioxane, and the excitation was set at 370 nm and the emission at 480 nm. The slit width of 10.0 nm for both excitation and emission wavelengths using a 3 mL quartz cuvette with a 10 mm path length and a magnetic stirrer. The anisotropy was calculated using equation 1. In this equation, I_{vv} and I_{vh} are fluorescence intensities measured using the polarizers' parallel and perpendicular geometry. The perpendicular components were corrected using the G factor ($G = I_{hv} / I_{hh}$) [3].

$$r = \frac{Ivv - G*Ivh}{Ivv + 2*G*Ivh} \quad (1)$$

2.4 Time-Resolved Fluorescence studies

The excited-state lifetimes were determined using a fixed concentration of the aminoquinoline (5.0 µM) in the presence or absence of DNA (50 µM) in 10 mM TRIS, pH 7.0, 25°C. The excitation was performed using a 450 ± 10 nm picosecond pulsed laser (EPL series, Edinburgh Instruments, Livingston, UK). The emission was measured using a 550 ± 25 nm interference filter. The measurements were performed using a Mini-tau filter-based

fluorescence lifetime spectrometer coupled to Time-Correlated Single Photon Counting (TCSPC) system (Edinburgh Instruments, Livingston, UK). The fluorescence decay profiles were fitted using the multiexponential decay equation (tail-fitting method, equation 2), and the average lifetime <τ> was calculated using equation 3. In these equations, τi is the lifetime of each component, and fi is the contribution of each component to total fluorescence decay. The quality of the fit was assessed by χ2 values and residuals [3].

$$I_T = \sum_{i=1}^{n} f_i e^{\frac{-T}{\tau_i}} \qquad (2)$$

$$< \tau >= \sum_{i=1}^{n} f_i \tau_i \qquad (3)$$

2.5 Circular dichroism studies

The effect of the aminoquinolines on the secondary structure of DNA was evaluated by circular dichroism. The experimental condition was DNA (100 μM) and aminoquinoline (10 μM) in 10 mM TRIS, pH 7.0, at 25°C. The experiments were performed using a spectropolarimeter equipped with a thermostatically controlled cell holder, 3 mL quartz cuvette with a 10 mm path length, and a magnetic stirrer (spectropolarimeter J-815, Jasco, Japan). The circular dichroism spectra were obtained with a scanning speed of 50 nm/min, 1 nm step resolution, and response time of 1 s. The baseline (TRIS) was subtracted from all measurements [4].

2.6 DNA melting studies

The melting temperature of DNA in the absence and presence of the aminoquinoline was determined by measuring the absorbance at 260 nm (spectropolarimeter, J-815, Jasco, Japan). The concentration of DNA (50.0 μM) and aminoquinoline (5.0 μM) were kept fixed, and the temperature was varied at 2°C/min (25 to 100°C). The ratio $(A-A_0)/(A_f-A_0)$ was plotted against the temperature from the absorbances. Where (A) is the absorbance value at each temperature, (A_0) is the initial absorbance, and (A_f) is the final absorbance [4].

2.7 Association constant and thermodynamic parameters

The association constant for the interaction of the aminoquinoline with DNA was performed by fluorescence spectroscopy. Aminoquinolines (0.1 µM) were titrated with DNA (0-150 µM) in 10 mM TRIS, pH 7.0, at 20°C and 40°C. The association constant (Ka) was calculated by fitting the experimental data into equation 4. In this equation, F_0, F, and F_c are the maximum fluorescence intensities in the absence, presence, and saturation concentration of DNA, respectively. [AQ] is the fixed concentration of aminoquinoline, and [DNA] is the variable concentration of DNA [5].

$$F_0 - F = \frac{[AQ]+[DNA]+K_d-\sqrt{([AQ]+[DNA]+K_d))^2-4[AQ][DNA]}}{2[AQ]} \times (F_0 - F_C) \quad (4)$$

The thermodynamic parameters were calculated based on the values of the association constant obtained at 20°C and 40°C and the application of the Van't Hoff equation 5. In this equation, K_2 and K_1 are the association constants obtained at T_1 and T_2, and ΔH° is the reaction enthalpy. The Gibbs free energy (ΔG°) and entropy (ΔS°) were obtained from equations 6 and 7 [5].

$$\Delta H^0 = \frac{ln\left|{}^{K_2}/_{K_1}\right| \times R}{\frac{1}{T_1}-\frac{1}{T_2}} \quad (5)$$

$$\Delta G° = -RTlnK \quad (6)$$

$$\Delta G° = \Delta H° - T\Delta S \quad (7)$$

2.8 Displacement studies (Minor groove versus intercalating ligands)

The binding site of aminoquinolines in DNA was characterized by comparing it with the well-established fluorescent probes of DNA, ethidium bromide, and Hoechst dye. Indomethacin, vanillin, and hydroxycoumarin were used as competitive ligands. The complexes formed by ethidium bromide (5.0 µM), Hoechst dye (5.0 µM), and aminoquinoline (5.0 µM) with DNA (100 µM) were titrated with indomethacin, vanillin, or 4-hydroxycoumarin (2.5 – 30 µM) in 10 mM TRIS, pH 7.0. The excitation was at 490 nm, and emission was in the range 530 – 600 nm

(aminoquinoline-DNA); 340 nm and 355 – 650 nm (Hoechst-DNA); 500 nm, and 530 – 700 nm (ethidium bromide-DNA). The ratio F_0/F was used to evaluate the relative displacement of the fluorescent probes [6].

2.9 Effect of ionic strength

The effect of ionic strength and the nature of metal ions on binding efficiency was carried out using sodium chloride (NaCl) and magnesium chloride ($MgCl_2$). The reaction medium was constituted of 10 mM Tris-HCl buffer, pH 7.0. DNA (100 μM) and aminoquinoles (5.0 μM) were titrated with NaCl (0-40 mM) or $MgCl_2$ (0-0.02 mM). For comparison, the experiment was also conducted using acridine orange (5 μM) instead of aminoquinolines. The spectral conditions were: Aminoquinoline-DNA (excitation 490 nm and emission 520 – 620 nm); acridine orange-DNA (excitation 495 nm and emission 505 – 620 nm) [7].

2.10 Molecular docking studies

The interaction between DNA and aminoquinolines was simulated by molecular docking using AutoDock 4.0 [8]. The crystal structure of DNA (PDB ID: 127D) [9] was obtained from Protein Data Bank. The molecular structures of aminoquinolines were prepared using ChemDraw 3D Pro. The DNA structure was prepared by removing water molecules using Discovery Studio Visualizer 2019. The addition of polar hydrogen atoms and allowed twists for the ligands in DNA were performed using AutoDock 4.0 tools. The parameters used during molecular docking were: The Lamarckian Genetic Algorithm, LGA, with a population size of 150. The other parameters were not changed. The grid spacing was 0.375 Å, centered at 15.002 (x); 21.23 (y); 8.452 (z), and the box sizes in the x, y, and z directions were 46, 52, and 120 points, respectively. The DNA structure was fixed in the molecular docking simulations, while the ligands were flexible. One hundred results were obtained for each molecular docking analysis showing different conformations. The cluster analysis of similar conformations was accomplished with

the RMSD of 2.0 Å. Conformations and interactions between the ligands and DNA were analyzed using Discovery Studio Visualizer.

2.11 Molecular dynamics

Ddd

3. Results and Discussion

3.1 Interaction of Aminoquinolines with DNA: General Features and pH effect

The aminoquinolines were prepared in our laboratory, and their synthesis and characterization are available in a recent publication [2]. Aminoquinolines are susceptible to solvatochromism, having their quantum yields increased and maxima of emission shifted to higher wavelengths [10]. Based on these spectroscopic features, we recently reported the application of aminoquinolines to determine the apparent dielectric constant in the albumin binding sites [2]. Here, we present a specific aminoquinoline that can be used as a fluorescent probe to study the interaction with the DNA.

Fig. 1A shows the molecular structures of the developed aminoquinolines, and Fig. 1B shows the fluorescence spectra of AQ4 in the presence and absence of DNA. Only AQ4, the aminoquinoline with a dimethylamine substituent, was sensitive to DNA (Fig. 1C). Indeed, the aminoquinolines (AQs) studies here are susceptible to medium polarity [2,11]. However, only AQ4 produced a specific emission band centered at 590 nm when excited at 490 nm in the presence of DNA (Fig. 1C).

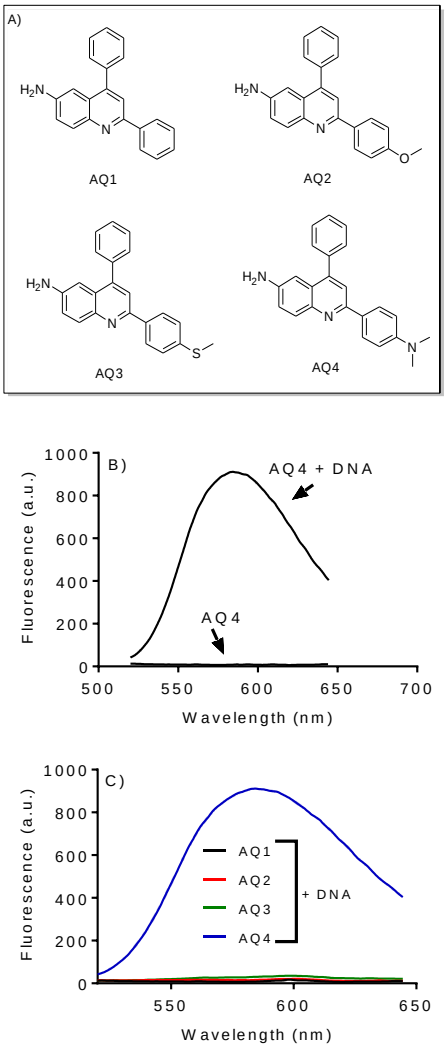

Fig. 1. (A) Molecular structure of aminoquinolines (AQs). (B) Emission spectra of AQ4 in the presence and absence of DNA. (C) Fluorescence of AQs in the presence of DNA. AQs 2.5 µM and DNA 25.0 µM, in 50 mM TRIS-HCl buffer, pH 7.0, 25°C, excitation at 490 nm.

This spectroscopic property of AQs in the presence of DNA is entirely different from that observed in organic solvents and is not related to solvatochromism. In organic solvents or complexed with albumin, the AQs present fluorescence maxima around 470 nm [2]. To demonstrate this feature, Fig. 2A depicts the emission spectra of AQ4 in solvents and compares them with that obtained by adding DNA. As can be seen, the emission maxima varied from 458 nm in nonpolar 1,4-dioxane to 495 nm when dissolved in the polar aprotic DMSO. In other

words, the solvatochromic susceptibility of the AQs cannot explain the wavelength shift caused by adding DNA (590 nm), i.e., almost 100 nm above the most polar solvent.

As the emission band observed in the presence of DNA was not related to medium hydrophobicity, the putative formation of an excited state complex (exciplex) was conceived. However, this hypothesis was discarded since the new fluorescence band was related to an also new absorption band. Fig. 2B shows a small but clear absorption band at 490 nm when DNA was present in the medium. This absorption band was still more intense at acidic pH, which had a prominent effect on fluorescence efficiency, as will be discussed later. Fig. 2C shows the excitation and emission spectra of AQ4 in the presence of DNA, reinforcing the formation of a new species absorbing at 490 nm. In short, the generation of a ground-state complex between DNA and AQ4 is the best candidate to explain the new red-shifted band.

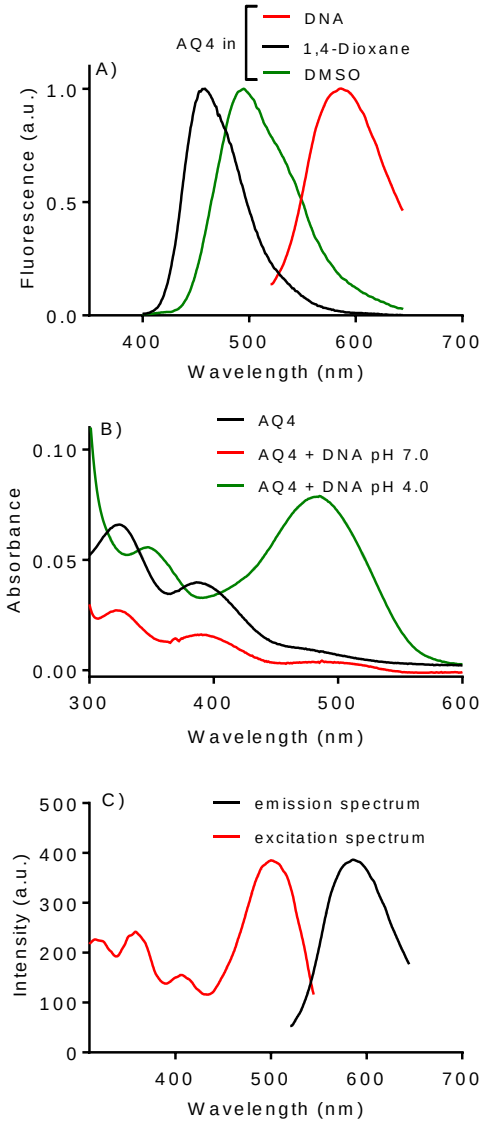

Fig. 2. Spectral features of AQ4 complexed with DNA: solvent effect versus DNA complexation. (A) Fluorescence spectra of AQs 2.5 µM dissolved in organic solvents or complexed with DNA (25 µM) in TRIS-HCl buffer, pH 7.0. (B) Absorption spectra in the presence and absence of DNA in 10 mM citrate pH 4.0 and 10 mM TRIS-HCl pH 7.0. (C) Excitation and emission spectra of AQ4 in the presence of DNA.

As described above, the medium pH plays a role in generating the complex between AQ4 and DNA. Hence, we advanced by measuring the relative fluorescence intensity in a broader pH range. The results in Fig. 3A confirmed the expectation since a higher fluorescence intensity was observed at acidic pH. Fig. 3B shows the fluorescence intensity ratio (+DNA/-DNA). At pH 4.0, the fluorescence was around 100-fold higher by adding DNA. In these experiments, aiming

to embrace the entire studied pH range, different buffers, with adequate pKa, were used. Hence, to exclude the putative effect of the various and different chemical constituents, in a separate experiment, only a buffer was used in the pH range of 5–7. The buffer MES (pKa 6.2) was adequate for this pH range. The higher fluorescence intensity was obtained at pH 5 (Fig. S1). In short, these findings showed that irrespective of the chemical nature of the medium, the pH is directly linked to the interaction between AQ4 and DNA. The importance of the medium pH made us question whether the other AQs could also present some fluorescence in a more acidic environment. Corroborant with our expectation, at pH 4.0, all studied AQs showed fluorescence after adding DNA (Fig. S2). Nevertheless, AQ4 was still the more efficient and selected for further studies. From a structural point of view and considering the pH effects, the presence of the dimethylamino substituent in AQ4 must be behind its improved susceptibility to DNA. It makes sense once its protonation could be the pathway for electrostatic interaction with the negatively charged DNA. Indeed, a typical chemical feature of many DNA probes is the presence of positively charged moieties. The cationic character usually improves the DNA binding affinity due to the increased electrostatic attraction between the probe and the DNA phosphates [12]. This property of AQ4 will be discussed later, along with the computational studies.

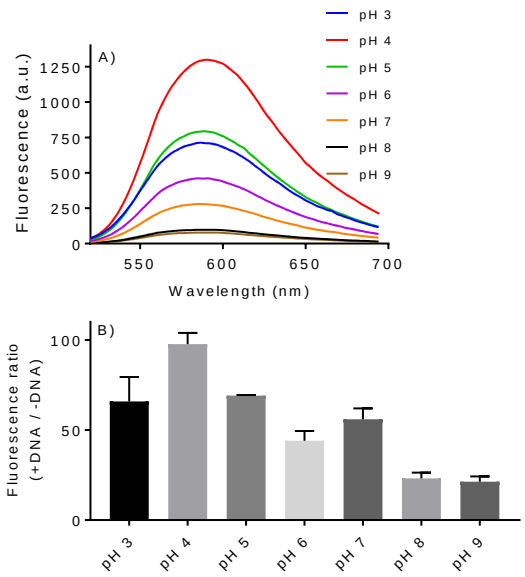

Fig. 3. pH effect on AQ4-DNA complex. (A) Fluorescence spectra at various pHs. (B) Fluorescence ratio (+DNA/-DNA) of AQ4 at different pHs. Experimental condition: AQs 2.5 µM with or without DNA (30 µM) in 10 mM buffers. pH 3.0-4.0 (formate), pH 5.0-6.0 (citrate), pH 7.0-9.0 (TRIS). The results are means and SD of triplicates.

3.2 Interaction AQ4 with DNA: Association pieces of evidence

The increased fluorescence of AQ4 due to adding DNA suggests binding. Hence, the next step was to gather additional experimental evidence of the complexation. Fig. 4A shows the effect of adding DNA to AQ4 regarding the lifetime of its excited state. As shown, the presence of DNA caused a four-fold increase in the excited AQ4 lifetime. This finding reinforces the binding of the fluorescent probe with DNA once the increased lifetime could result from the suppression of non-radiative pathways linked to thermal relaxation. This biophysical feature can be explained by the restriction associated with the protein microenvironment, membranes, and nucleic acids [3,13–15]. In other words, the AQ4 mobility complexed with DNA was significantly reduced. Corroborant with these findings, increased lifetimes have been reported for 8-anilino-1-naphthalene sulfonate [16] and *N,N*-dimethylaminobenzophenone [17] interacting with DNA.

In line with the previous findings, the fluorescence anisotropy of AQ4 was also dramatically increased by adding DNA. As well-known, fluorescence anisotropy is an effective tool for

identifying molecular interactions. Fluorescence anisotropy depends on the rotational diffusion of the fluorophore and is also considered a sensitive indicator for monitoring ligand binding to macromolecular systems. As shown, the addition of DNA to AQ4 caused a significant increase in fluorescence anisotropy (Fig. 4B). Indeed, the observed anisotropy (0.29) was almost the maximum that can be obtained for this biophysical parameter (0.33) [3]. This result agrees with those reported for minor groove stains Hoechst [18] and DAPI [19]. For comparison, Fig. 4B also shows the anisotropy of AQ4 free in solution. In this case, the measurements were performed with AQ4 dissolved in 1,4-dioxane once it was not fluorescent when free in the aqueous medium. As shown, in the absence of DNA, the fluorescence from free AQ4 was devoid of anisotropy due to the rapid tumbling motion of the probe in bulk medium.

The previous findings strongly suggest complexation; hence an immediate question is whether the interaction is intercalative or groove binding mode. In this concern, two experiments were performed. The first one was by measuring the effect of AQ4 in the intrinsic CD spectrum of DNA. As well-established, the secondary structure of DNA is altered by the intercalation of small ligands, which can be detected by CD. Conversely, the typical signature of DNA-groove interaction is the absence of alteration [20]. Fig. 4C shows the CD spectrum of DNA in TRIS buffer at pH 7.0. The complexation did not alter the intrinsic positive peak at 275 nm and the negative at 245 nm, which are the typical values of calf thymus DNA [21]. In short, the binding of AQ4 did not disturb the stacking of the bases in DNA.

Another typical spectroscopic feature of a DNA-groove interaction is the absence of significant alteration in the melting point of DNA. Fig. 4D shows the temperature-dependent absorption change of DNA at 260 nm. As can be seen, a typical sigmoidal curve (cooperative process) was obtained due to the unfolding of the double-helical DNA strands into single strands. The absorbance increase because the extinction coefficient of DNA bases at 260 nm in the double-helical form is much less than in the single-stranded form. The melting temperature was

80.3°C, which is close to 78.7°C [22] and 85.0°C [23], both were recently reported to ct-DNA, which was used throughout this study. As shown, the presence of AQ4 did not alter the melting temperature (Fig 4D). Compared with other DNA probes, this result reinforces the non-intercalative feature of AQ4. Indeed, the intercalation of small molecules into the double helix is known to alter the helix melting temperature, whereas minor groove ligands typically are non-effective [24–26].

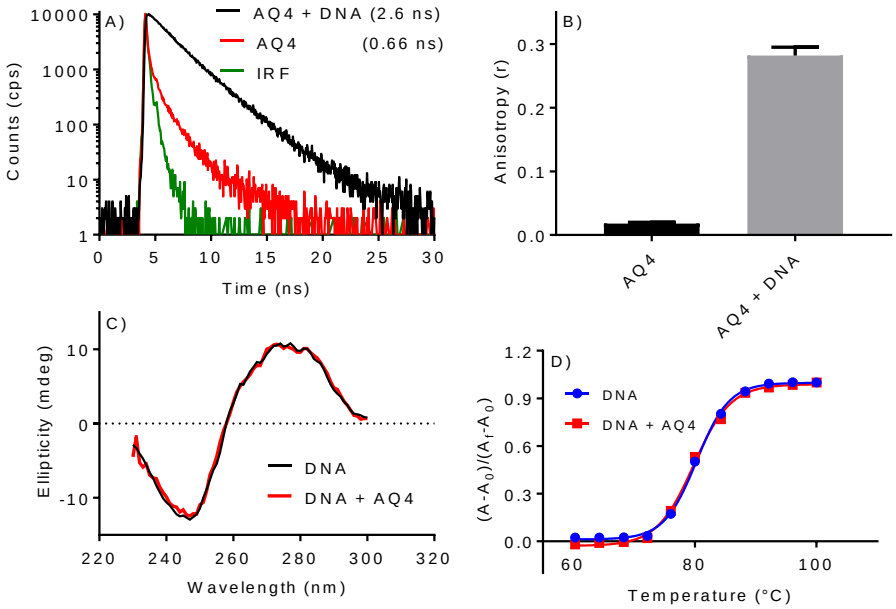

Fig. 4. Spectroscopic evidence of the complexation between AQ4 and DNA. A) Effect of DNA on the lifetime of excited AQ4. B) Effect of DNA on fluorescence anisotropy of AQ4. C) Effect of AQ4 on intrinsic CD spectrum of DNA. D) Effect of AQ4 in the melting point of DNA.

3.3 Association constant and thermodynamic parameters

Once AQ4 acts as a ligand of DNA, the next step was to determine its association constant. To do so, we used the fluorescence band generated by the interaction. Fig. 5A shows the fluorescence increase caused by the titration of AQ4 with DNA. The excitation was performed at 490 nm, where DNA is entirely transparent; hence there was no spectroscopic interference in the measurement. The progressive fluorescence increase and saturation are typical features of

complexation (Fig. 5A). The association constants were obtained using a nonlinear fitting model (equation 4). Fig. 5B shows the excellent fit obtained at two temperatures. Table 1 shows the obtained association constants.

A comparison with other ligands can be elucidative to indicate the binding mode. Some examples, divided by type of interaction, are the following. **i)** Reported as intercalative ligands: 9-anthrylmethyl)ammonium chloride (7.8 x 10^4 M^{-1}) [12]; quinoline derivatives (10^4 to 10^6 M^{-1} [27]; bifenthrin (10^4 M^{-1}) [28]; carbazolyl porphyrins (10^5 M^{-1}) [29]. **ii)** Reported as minor groove ligands: febuxostat, an inhibitor of xanthine oxidase (0.9x 10^3 M^{-1}) [30] ; cyanine (3.4x10^3 M^{-1}) (10.26565/2312-4334-2019-3-08); elmisartan, an angiotensin II ligand (2.7 x 10^3 M^{-1}) (10.1016/j.molliq.2018.06.057); anticancer compound luotonin (2.2 x 10^2 M^{-1}) [31]. Comparing these reported binding constants and the obtained here (6.3 x 10^3 M^{-1}, Fig. 5 and Table 1), it can be supposed that an external non-intercalative mode is the most probable to AQ4.

Based on the determination of the association constants at two different temperatures, the thermodynamic parameters were calculated according to Van't Hoff and Gibbs equations (equations 5-7). The values of ΔG° were found to be negative at all temperatures, highlighting the feasibility of interaction. The negative values for both ΔH° and Δ°S suggest that van der Waals forces and hydrogen bonding are the main driven force for the interaction [32]. Similar results were reported for other minor groove ligands such as R,S-venlafaxine hydrochloride [33], isoflavones [4], caffeic acid [34], and pioglitazone, an oral antidiabetic [6].

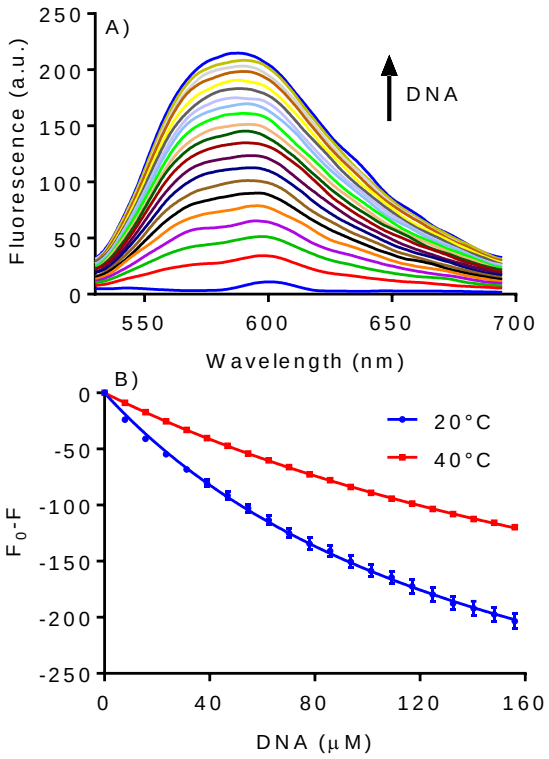

Fig. 5. Determination of association constants between AQ4 and DNA. A) Spectral alteration of AQ4 caused by titration with DNA. B) Fit of the experimental data on Eq. 4. The experiments were performed in 10 mM TRIS-HCl buffer pH 7.0 at 20 and 40C. The results as means and SD of triplicates

Table 1. Association constants and thermodynamic parameters for the interaction DNA-AQ4

	Ka x 10^3 (mol^{-1} L)	**ΔG° (kJ mol^{-1})**	**ΔH° (kJ mol^{-1})**	**ΔS° (J mol^{-1} K^{-1})**
20°C	6.3 ± 0.1	-21.2	-23.3	-7.1
40°C	3.3 ± 0.2	-21.1		-7.1

3.4 Effect of ionic strength

In the previous sections, we have shown that the interaction of AQ4 did not cause alteration in the secondary structure of the nucleic acid, i.e., the intrinsic CD spectrum and melting temperature of DNA were not altered by complexation with AQ4. These features are usually associated with non-intercalating probes [20]. Hence, the second option is the interactions in the grooves of the nucleic acid and/or external binding of electrostatic nature.

Pursuing this hypothesis, competitive displacement experiments were performed here and in the following sections.

The first one was to evaluate the effect of ionic strength in the interaction of AQ4 with DNA, which is a well-established method to distinguish the binding mode between molecules and DNA. The theoretical background of this experimental approach is the shielding effect obtained at high ionic strength that reduces the electrostatic repulsion between the negatively charged phosphate backbone on adjacent nucleotides. Commonly, NaCl at high concentration is employed once the electrostatic interaction is decreased in the presence of Na^+ ions leading to DNA chain shrink. The typical result is a decrease in the binding efficiency of ligands to DNA. It is the case of interactions in the surface of DNA, as minor groove interactions and electrostatic force involving the anionic phosphate backbone of DNA. On the other hand, intercalative ligands are less susceptible to ionic strength [35]. Based on this well-established knowledge, we studied the displacement of AQ4 from DNA by increasing the concentration of NaCl. In addition, we used acridine orange (AO) as a control for the effect of the ionic strength in a typical intercalative fluorescent DNA probe [36]. Fig. 6 shows the displacement of AQ4 and AO due to the increase in the medium ionic strength. The relative displacement efficiency was measured by the Stern-Volmer fluorescence quenching constant (Ksv) (Fig. 6C). From the obtained constants for AQ4 (86.3±0.3 M^{-1}) and AO (1.3±0.4 M^{-1}), it can be deduced that AQ4 is not an intercalating probe, which agrees with the melting temperature and CD studies. In addition, this finding suggests that AQ4 was released from DNA by increased ionic strength, showing that electrostatic interaction plays a significant role in the complexation process. A similar result was reported for edifenphos, an organophosphate pesticide [37], and florfenicol, a broad-spectrum antibacterial drug [38]. These drugs were reported as minor groove ligands. It is worth noting that the electrostatic effect is often observed as an auxiliary in assisting groove binding and intercalation. As reported, small molecules that bind strongly to DNA are usually accompanied by the electrostatic component [39].

3.5 Effect of Magnesium ion

Besides an unspecific electrostatic effect related to ionic strength, metal ions directly affect DNA conformation. Indeed, as a supercoiled negatively charged polymer of nucleotide units, DNA interacts directly with positively charged metal ions. These interactions are crucial for the conformational structure and functions of these biomacromolecules. The sites of interaction on DNA are the negatively charged phosphates of the backbone of both strands and the electron donor atoms of the bases, such as N and O of the nucleobases, for instance, the N7 and O6 of guanine and N7 and N1 of adenine bases and the N3 of pyrimidines [40,41]. Among these metal ions, Mg^{+2} ion has a central role once it is the primary intracellular divalent ion and is present in all DNA and RNA activation processes. The greater charge density is behind the more tightly binding capacity of Mg^{+2} than Na^{+} [42]. In addition, it was shown that increasing Mg^{+2} ions concentration changes the B-DNA form to Z-DNA. Based on these features of Mg^{+2} ions, we tested their effect on AQ4 interaction. The results in Fig. 6 agree with the expected role of Mg^{+2} ions on DNA. As can be seen, the interaction was at least two orders of magnitude higher compared to Na^{+} ions. As shown, using $MgCl_2$, the Stern-Vomer quenching constant was 4.1 x 10^4 M^{-1}, while only 86.3 M^{-1} for NaCl (Fig. 5). Moreover, the displacement of AQ4 was much more susceptible to Mg^{+2} compared to the intercalating AO (Ksv 0.6 x 10^4 M^{-1}), confirming that AQ4 is not an intercalating ligand.

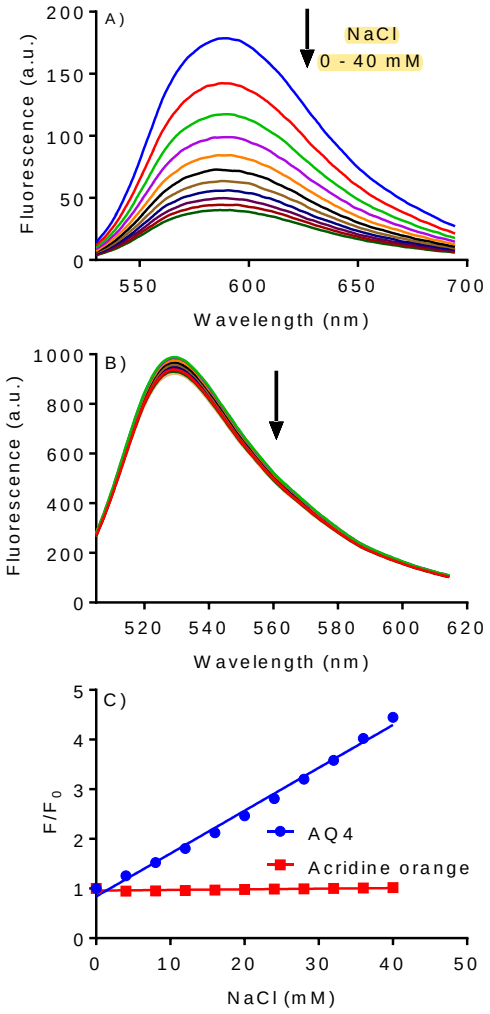

Fig 6. Effect of NaCl on AQ4-DNA and comparison with acridine orange-DNA. (A) Fluorescence quenching of AQ4-DNA by adding NaCl. (B) Fluorescence quenching of acridine orange/DNA by adding NaCl. (C) Stern-Volmer plots AQ4-DNA (Ksv: 86.3 M^{-1}), acridine orange-DNA (Ksv: 1.3 M^{-1}). AQ4 and acridine orange (5 µM), DNA (100 µM in 10 mM TRIS-HCl buffer, pH 7.0.

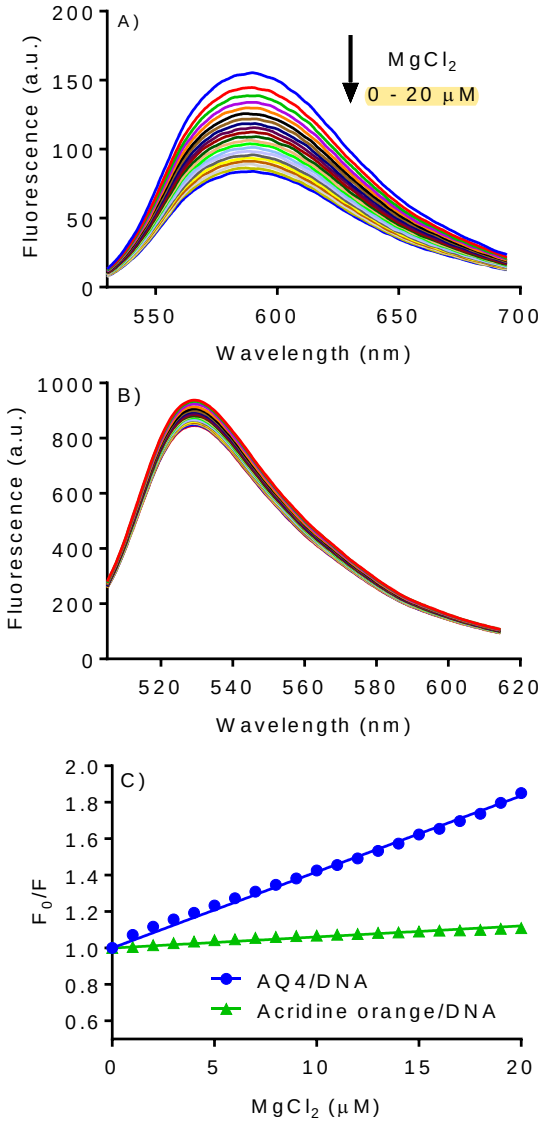

Fig 7. Effect of $MgCl_2$ on AQ4-DNA and comparison with acridine orange-DNA. (A) Fluorescence quenching of AQ4-DNA by adding $MgCl_2$. (B) Fluorescence quenching of acridine orange-DNA by adding $MgCl_2$. (C) Stern-Volmer plots AQ4-DNA (Ksv: 4.1 x 10^4 M^{-1}), acridine orange-DNA (Ksv: 0.6 x 10^4 M^{-1}). AQ4 and acridine orange (5 µM), DNA (100 µM in 10 mM TRIS-HCl buffer, pH 7.0.

3.6 Effect of Norfloxacin

Norfloxacin is a quinolone antibiotic with a broad antibacterial spectrum and is extensively used in treating infectious diseases [43]. Quinolones are antibacterial agents that inhibit DNA replication and are commonly used to treat many infections. Norfloxacin is a potent DNA gyrase inhibitor, and the mechanism of action is related to DNA interaction [44]. Regarding

DNA binding, there is solid evidence of norfloxacin as a minor groove ligand. For instance, the interaction of norfloxacin with the DNA oligonucleotide d[ATATCGATAT] was investigated by molecular dynamics and revealed that norfloxacin was inserted in the minor groove of DNA, binding to the region of duplex TCGA bases [45]. Similarly, Linus et al. propose a nonintercalative mode of interaction since the drug binds preferentially to single-stranded DNA rather than to double-stranded DNA [44]. Vijan et al., using ct-DNA, proposed two types of interaction. An internal binding process implying the drug intercalation between base pairs of DNA, and an external binding process, suggesting the binding of the drug in the grooves from the nucleic acid structure. However, the predominant was the external binding, which presented a binding constant of one order of magnitude higher [46]. Based on the above literature data, it can be concluded that the predominant mode of binding of norfloxacin is in the DNA groove. Our results agree with these findings. Indeed, norfloxacin was able to remove the intercalating AO (Ksv: 2.2 x 10^2 M^{-1}), but the efficiency was significantly lower than AQ4 (Ksv 1.3 x 10^4 M^{-1}), reinforcing its minor groove feature (Fig. 8).

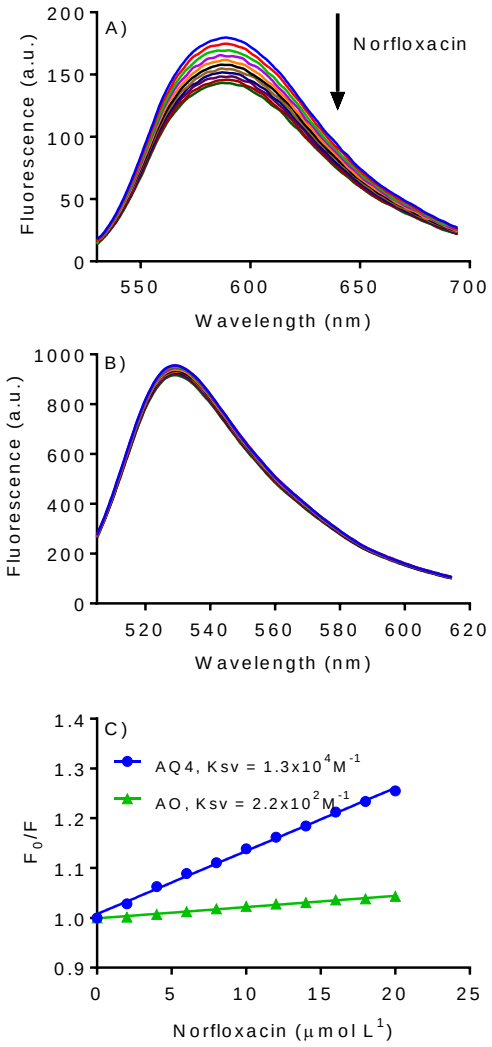

Fig 8. Effect of norfloxacin and comparison with acridine orange. (A) Fluorescence quenching of AQ4-DNA by adding norfloxacin. (B) Fluorescence quenching of acridine orange-DNA by adding norfloxacin. (C) Stern-Volmer plots AQ4-DNA (Ksv: 1.3 x 10^4 M^{-1}), acridine orange-DNA (Ksv: 2.2 x 10^2 M^{-1}). AQ4 and acridine orange (5 µM), DNA (100 µM in 10 mM TRIS-HCl buffer, pH 7.0.

3.7 Comparison with minor groove and intercalating commercial dyes

The previous findings strongly suggest that AQ4 acts as a minor groove ligand. Hence, to reinforce this biophysical feature, its performance was compared with fluorescent probes widely used to characterize the mode of interaction of new and developing drugs with DNA. The choice was the Hoechst 33258 (HO) stain, which is a cell-permeant nuclear dye that emits blue fluorescence when bound to DNA [47], and ethidium bromide (EtBr), an intercalating agent

commonly used as a nucleic acid stain [48]. HO is a widely used minor groove stain that binds preferentially to the AT-rich region of double-stranded DNA with a minimum of four consecutive AT base pairs [49–51]. EtBr binds to double-stranded DNA by intercalative mode by inserting planar aromatic rings between the DNA base pairs [48]. Fig. 9 depicts and compares AQ4, HO, and EtBr emission spectra. The experiments were performed in the same concentration of DNA and dyes and with the same fluorimeter setup, including attenuation filters and photomultiplier voltage. The only difference was the excitation wavelengths. Based on the spectra, it is evident that EtBr and HO have a higher fluorescence efficiency compared to AQ4. However, considering the fluorescence ratio, i.e. +DNA/-DNA, the following values were obtained by measuring the AUC of the fluorescence spectra: AQ4 (66.8), HO (11.1) and EtBr (3.7). This was due to the total absence of fluorescence of AQ4 free in solution (Fig. 9). In other words, AQ4 presented a higher sensitivity to detect DNA compared to AQ and EtBr. Another potential advantage of AQ4 is the excitation and emission wavelengths range. The excitation with green light (500 nm) would not be harmful for living cells. Indeed, this is an issue for utilization of 4’,6-diamidino-2-phenylindole (DAPI), one of the most used DNA stains. DAPI is excited in the UV range (358 nm), hence detecting live samples with DAPI can lead to cell death, which limits the accessible observation time [52]. Fig. 9 shows shots of the cuvette containing AQ4, HO and EtBr in the presence of DNA.

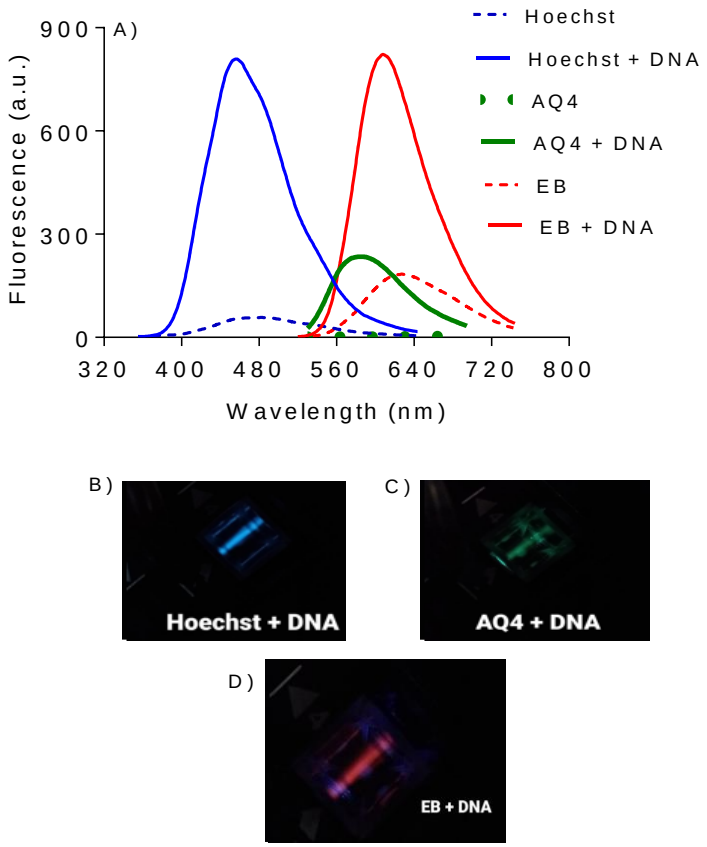

Fig 9. Spectral features: AQ4 versus Hoechst versus Ethidium bromide. (A) Fluorescence spectra in the presence and absence of DNA. (B,C,D) shots of the cuvette highlighting the color of the probes complexed with DNA. Experimental condition: AQ4, Hoechst and ethidium bromide (5 µM), DNA (100 µM) in 10 mM TRIS-HCl buffer, pH 7.0. The excitations were performed at 490 nm (AQ4), 340 nm (Hoechst), and 500 nm (Ethidium bromide).

To compare the DNA binding features of AQ4 with EtBr and HO, we selected three drugs that have been studied as DNA ligands. The first was the food additive and flavor enhancer vanillin, which has several biological effects and interactions with proteins [53,54]. Regarding interaction with DNA, Xia et al. showed that vanillin acts as a minor groove ligand. The conclusion was supported by viscosity measurements, melting studies, denaturation experiments, and competitive binding investigations [55]. Fig. 10A shows the Stern-Volmer plot of the quenching effect of vanillin on the complexes AQ4-DNA, HO-DNA, and EtBr-DNA. As can be seen, and in agreement with the reported study, vanillin was more effective in the displacement of HO.

Furthermore, corroborating our previous studies, the removal of AQ4 was also effective, reinforcing its minor groove character.

The second drug used to validate AQ4 as a minor groove ligand was indomethacin, a potent non-steroidal anti-inflammatory drug [56]. Besides its well-established mechanism of action as a cyclooxygenase inhibitor, other pharmacological actions and applications have emerged for indomethacin, including antiviral effects [57]. Husain et al. studied its mode of interaction with DNA and got evidence of the complexation with nucleic acid. Again, applying displacement studies with AO and HO, among other models, the authors concluded that indomethacin is a minor groove ligand [58]. Fig. 10B shows the Stern-Volmer plot of the quenching effect of indomethacin on the complexes AQ4-DNA, HO-DNA, and EtBr-DNA. As shown, the displacement caused by indomethacin upon the complex AQ4-DNA is in total agreement with the expected for a minor groove ligand.

The third drug used was 4-hydroxycoumarin. Coumarins are compounds that have been extensively studied for their diverse pharmacological properties. Among them is warfarin, a well-known anticoagulant agent [59]. In this line of investigation, Sarwar et al. proposed that coumarin is also a minor groove ligand [60]. Based on the reported experimental evidence, we used 4-hydroxycoumarin to test its capacity to displace AQ4. The result was consistent with the previous one, reinforcing that AQ4 is a minor groove ligand (Fig. 10C).

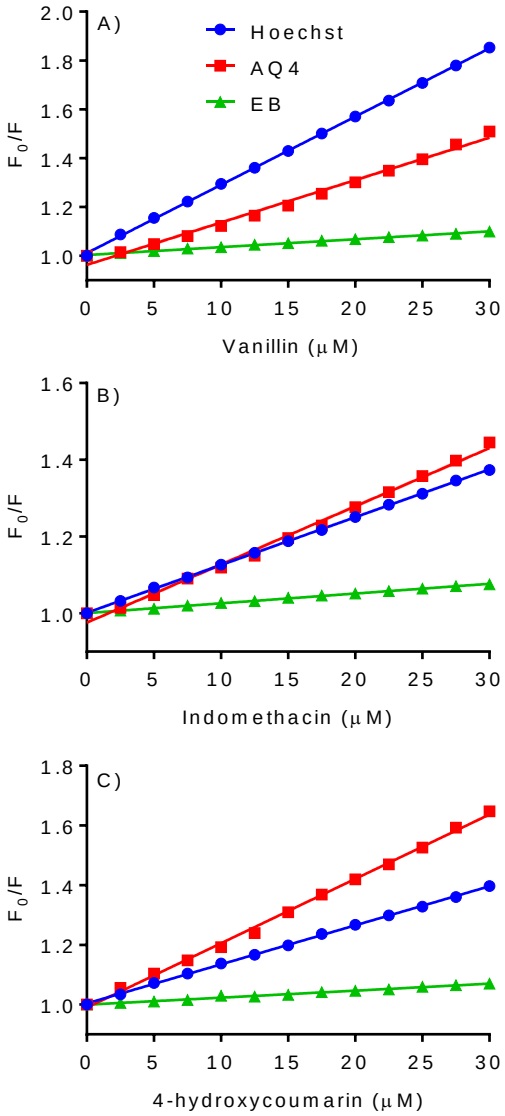

Fig. 10. AQ4, Hoechst, and ethidium bromide: Intercalative versus minor groove. Comparative displacement effect caused by (A) Vanillin, (B) indomethacin, and (C) 4-hydroxycoumarin. Experimental condition: Fluorescent dyes (5 μM), DNA (100 μM) in 10 mM TRIS-HCl buffer, pH 7.0.

3.8 Molecular docking: Comparing AQ4 with Hoechst 33258

The previous findings strongly suggest that AQ4 is a minor groove ligand. However, the weakening of interaction due to the increase in ionic strength of the medium also indicates that a nonspecific electrostatic interaction might play an important role in the interaction. Thus, to advance in the comprehension of the mechanism of complexation, molecular docking

calculations were performed to determine the docking poses and to reveal the possible interactions between AQ4 and DNA.

Considering that AQ4 was compared with HO in our experimental studies, we followed the same approach in the computational ones. To do so, the crystallographic structure of the DNA dodecamer d(CGC[e6G]AATTCGCG) complexed with the minor groove ligand HO was used for comparison [9]. Fig. 11 depicts the structure of the complex (PDB ID: 127D) prepared using the Discovery Studio Visualizer software and highlighted the interaction of HO dye with the AATT region in the minor groove.

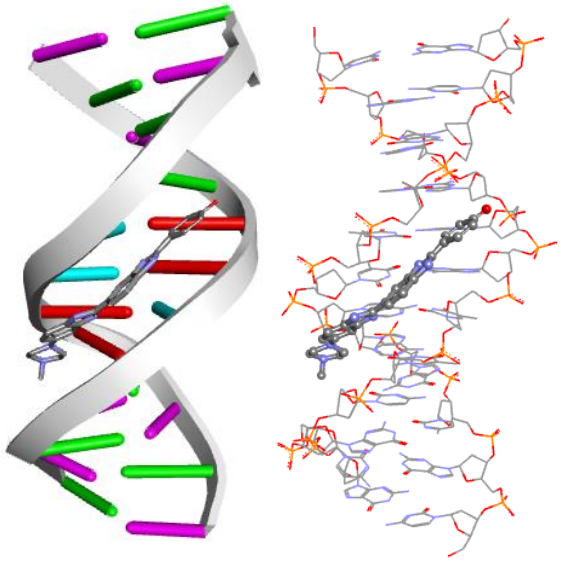

Fig. 11. Crystallographic structure of the DNA dodecamer d(CGC[e6G]AATTCGCG) complexed with minor groove ligand Hoechst (PDB ID: 127D, 10.1002/j.1460-2075.1992.tb05045.x). The nucleobases are adenine (red), thymine (blue), guanine (green) and cytosine (purple). The figure was prepared using the Discovery Studio Visualizer software.

Then, HO was removed, and AQ4 was docked in the DNA dodecamer. To do so, the selected grid box in AutoDock4 tools enclosed the entire DNA dodecamer. Hence, AQ4 was free to interact in the DNA in any location (Fig Sx). However, corroborating our expectations, the minor groove region was preferential. The simulation resulted in six pose clusters, all localized close to the area occupied by the HO in the crystallographic structure (Table 2). Figs. 12A and 12B show the lowest energy pose of each cluster. Fig. 12C and Table 3 show the interactions with the

nucleobases. An important finding was the detection of electrostatic interaction, with is consistent with the experimental susceptibility to ionic strength. Fig. 13 shows the superposition of the lowest energy pose of the most populated cluster (11.94 kcal mol^{-1}, 75%) of AQ4-DNA with the crystallographic structure HO-DNA. In short, the computational simulations were consistent with our experimental data, showing that AQ4 can bind in the minor groove region of DNA.

Table 2. Pose clusters for the interaction AQ4-DNA dodecamer (PDB ID: 127D). Protonated and deprotonated forms.

	Cluster Rank	**Lowest Binding Energy (kcal mol^{-1})**	**Mean Binding Energy (kcal mol^{-1})**	**Number in the cluster (%)***
$AQ4(H^+)$	1	-11,94	-11,85	75
	2	-10,48	-10,47	2
	3	-10,40	-10,13	9
	4	-10,36	-10,17	7
	5	-10,12	-10,12	1
	6	-9,01	-8,98	6
AQ4	1	-9,61	-9,54	79
	2	-9,18	-8,99	6
	3	-8,77	-8,71	2
	4	-8,52	-8,52	1
	5	-8,51	-8,47	3
	6	-8,11	-8,05	6
	7	-8,04	-8,04	1
	8	-7,61	-7,60	2

*RMSD: 2,0 Å

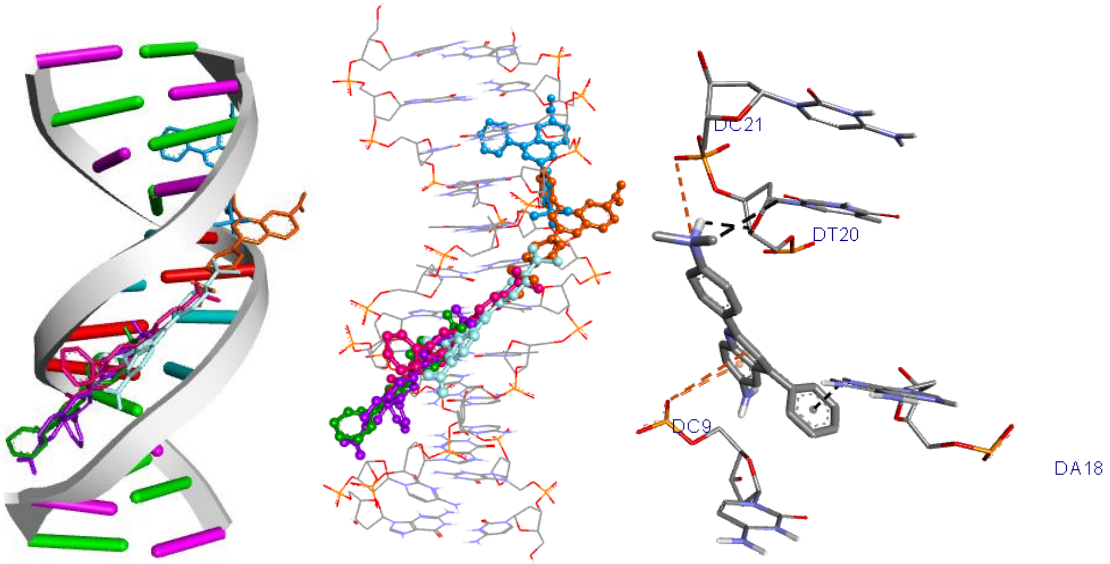

Fig. 12. AQ4 docked in DNA dodecamer d(CGC[e6G]AATTCGCG) PDB ID: 127D. (A,B) The six lower energy poses of each cluster. (C) Intermolecular interaction with nitrogenous bases.

Table 3. Interaction with nucleobases: complex AQ4-DNA dodecamer (PDB ID: 127D). Protonated and deprotonated forms.

	Nucleobase	**Interaction**	**Distance (Å)**
AQ4(H^+)	DC21	electrostatic	5,51
	DT20	hydrogen bond	2,42
	DT20	hydrogen bond	3,29
	DC9	electrostatic	3,96
	DC9	electrostatic	4,77
	DA18	hydrogen bond	2,97
AQ4	DC20	hydrogen bond	3,23
	DT7	hydrogen bond	3,13
	DT20	electrostatic	4,76
	DA18	hydrogen bond	3,04

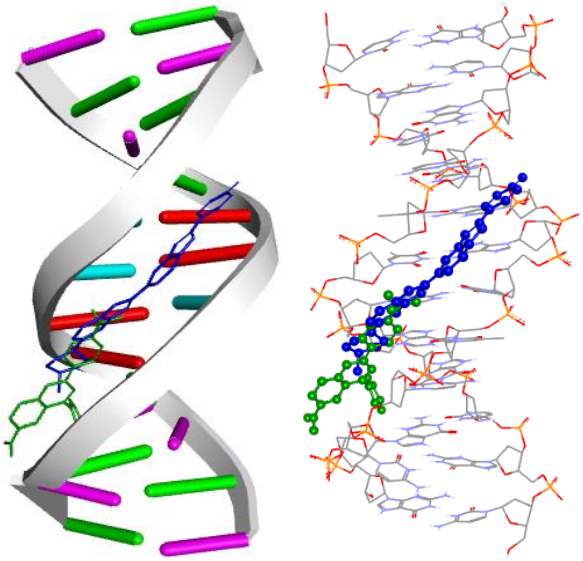

Fig. 13. Superposition of lower energy of the most populated cluster of AQ-DNA and the crystallographic structure HO-DNA dodecamer d(CGC[e6G]AATTCGCG) PDB ID: 127D.

3.8.1 Protonated versus deprotonated AQ4

As noted in section 3.1, the medium pH significantly affected AQ4 binding, which is more favorable at acidic pH. As also highlighted, the difference among the aminoquinolines studied that favored AQ4 is the presence of the $N(CH3)_2$ substituent. Thus, it can be conceived that its protonation might be involved in the binding with DNA. Scheme 1 shows the equilibrium equation for the protonation of AQ4. There are other sites of protonations, but as $N(CH3)_2$ is responsible for the efficiency of AQ4, it was the only one considered. Its pKa was obtained by simulation and resulted in 3.91 (MarvinSketch, ChemAxon 21.14). Hence, a significant proportion of protonation must occur in the pH range of 4 – 5.

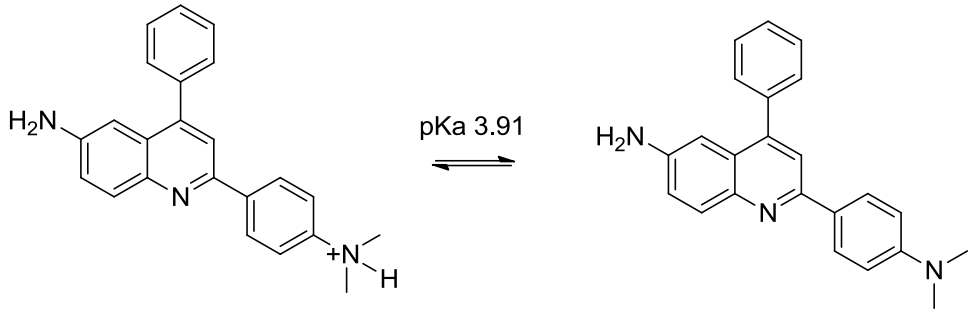

Scheme. 1. Protonated and deprotonated forms of AQ4.

Based on these considerations, the docking simulation was also performed with the deprotonated form of AQ4. Table 2 depicts the clusters and binding energies. As can be seen, the energies were consistently lower for the protonated form, which agrees with the experimental data. The involvement of a protonated form of AQ4 could also explain the strong effect of the ionic strength (Fig. 6). It could be involved in the electrostatic interaction between AQ4 and DNA. Indeed, comparing the interactions with the nucleobases, the electrostatic interactions are prevalent for the protonated form compared to the deprotonated one (Table 3).

Conclusion

References

[1] Shahabadi N, Hadidi S. Spectroscopic studies on the interaction of calf thymus DNA with

the drug levetiracetam. Spectrochim Acta Part A Mol Biomol Spectrosc 2012;96:278–83. https://doi.org/10.1016/J.SAA.2012.05.045.

[2] Pastrello B, dos Santos GC, Silva-Filho LC da, de Souza AR, Morgon NH, Ximenes VF. Novel aminoquinoline-based solvatochromic fluorescence probe: Interaction with albumin, lysozyme and characterization of amyloid fibrils. Dye Pigment 2020;173. https://doi.org/10.1016/j.dyepig.2019.107874.

[3] Lakowicz JR. Introduction to Fluorescence. Princ. Fluoresc. Spectrosc., Boston, MA: Springer US; 2006, p. 1–26. https://doi.org/10.1007/978-0-387-46312-4_1.

[4] Pawar S, Tandel R, Kunabevu R, Jaldappagari S. Spectroscopic and computational approaches to unravel the mode of binding between a isoflavone, biochanin-A and calf thymus DNA. J Biomol Struct Dyn 2019;37:846–56. https://doi.org/10.1080/07391102.2018.1442748.

[5] Fernandes AJFC, de Carvalho Bertozo L, Povinelli APR, Zazeri G, de Souza AR, Morgon NH, et al. 4-Dimethylamino-beta-nitrostyrene, a fluorescent solvatochromic probe to estimate the apparent dielectric constant in serum albumin: Experimental and molecular dynamics studies. J Photochem Photobiol A Chem 2022;433:114197. https://doi.org/10.1016/J.JPHOTOCHEM.2022.114197.

[6] Al Qumaizi KI, Anwer R, Ahmad N, Alosaimi SM, Fatma T. Study on the interaction of antidiabetic drug Pioglitazone with calf thymus DNA using spectroscopic techniques. J Mol Recognit 2018;31:e2735. https://doi.org/10.1002/JMR.2735.

[7] Magdy G, Belal F, Abdel Hakiem AF, Abdel-Megied AM. Salmon sperm DNA binding study to cabozantinib, a tyrosine kinase inhibitor: Multi-spectroscopic and molecular docking approaches. Int J Biol Macromol 2021;182:1852–62. https://doi.org/10.1016/J.IJBIOMAC.2021.05.164.

[8] Morris GM, Huey R, Lindstrom W, Sanner MF, Belew RK, Goodsell DS, et al. AutoDock4 and AutoDockTools4: Automated docking with selective receptor flexibility. J Comput Chem 2009;30:2785–91. https://doi.org/10.1002/jcc.21256.

[9] Sriram M, Van der Marel GA, Roelen HLPF, Van Boom JH, Wang AHJ. Conformation of B-DNA containing O6-ethyl-G-C base pairs stabilized by minor groove binding drugs: molecular structure of d(CGC[e6G]AATTCGCG complexed with Hoechst 33258 or Hoechst 33342. EMBO J 1992;11:225–32. https://doi.org/10.1002/J.1460-2075.1992.TB05045.X.

[10] Santos GC, de Andrade Bartolomeu A, Ximenes VF, da Silva-Filho LC. Facile Synthesis and Photophysical Characterization of New Quinoline Dyes. J Fluoresc 2017;27. https://doi.org/10.1007/s10895-016-1954-5.

[11] Dos Santos GC, Servilha RO, de Oliveira EF, Lavarda FC, Ximenes VF, da Silva-Filho LC. Theoretical-Experimental Photophysical Investigations of the Solvent Effect on the Properties of Green- and Blue-Light-Emitting Quinoline Derivatives. J Fluoresc 2017. https://doi.org/10.1007/s10895-017-2108-0.

[12] Kumar C V., Asuncion EH. DNA Binding Studies and Site Selective Fluorescence Sensitization of an Anthryl Probe. J Am Chem Soc 1993;115:8547–53. https://doi.org/10.1021/JA00072A004/SUPPL_FILE/JA8547.PDF.

[13] Klymchenko AS. Solvatochromic and Fluorogenic Dyes as Environment-Sensitive Probes: Design and Biological Applications. Acc Chem Res 2017;50:366–75.

https://doi.org/10.1021/ACS.ACCOUNTS.6B00517/ASSET/IMAGES/LARGE/AR-2016-005173_0010.JPEG.

[14] Mudliar NH, Pettiwala AM, Awasthi AA, Singh PK. On the Molecular Form of Amyloid Marker, Auramine O, in Human Insulin Fibrils. J Phys Chem B 2016;120:12474–85. https://doi.org/10.1021/ACS.JPCB.6B10078.

[15] Bertozo LDC, Maszota-Zieleniak M, Bolean M, Ciancaglini P, Samsonov SA, Ximenes VF. Binding of fluorescent dansyl amino acids in albumin: When access to the protein cavity is more important than the strength of binding. Dye Pigment 2021;188. https://doi.org/10.1016/j.dyepig.2021.109195.

[16] Ghosh S, Kundu P, Paul BK, Chattopadhyay N. Binding of an anionic fluorescent probe with calf thymus DNA and effect of salt on the probe–DNA binding: a spectroscopic and molecular docking investigation. RSC Adv 2014;4:63549–58. https://doi.org/10.1039/C4RA14298E.

[17] Schweigert C, Gaß N, Wagenknecht HA, Unterreiner AN. Significant Fluorescence Enhancement of N,N-Dimethylaminobenzophenone after Embedding as a C-Nucleoside in DNA. ChemPhotoChem 2018;2:12–7. https://doi.org/10.1002/CPTC.201700183.

[18] Banerjee D, Pal SK. Simultaneous binding of minor groove binder and intercalator to dodecamer DNA: Importance of relative orientation of donor and acceptor in FRET. J Phys Chem B 2007;111:5047–52. https://doi.org/10.1021/JP0715427/ASSET/IMAGES/LARGE/JP0715427F00005.JPEG.

[19] Banerjee D, Pal SK. Dynamics in the DNA recognition by DAPI: Exploration of the various binding modes. J Phys Chem B 2008;112:1016–21. https://doi.org/10.1021/JP077090F/ASSET/IMAGES/LARGE/JP077090FF00005.JPEG.

[20] Sha Y, Chen X, Niu B, Chen Q. The Interaction Mode of Groove Binding Between Quercetin and Calf Thymus DNA Based on Spectrometry and Simulation. Chem Biodivers 2017;14:e1700133. https://doi.org/10.1002/CBDV.201700133.

[21] Huang S, Luo H, Liu Y, Su W, Xiao Q. Comparable investigation of binding interactions between three arene ruthenium(II) thiosemicarbazone complexes and calf thymus DNA. Polyhedron 2020;192:114864. https://doi.org/10.1016/J.POLY.2020.114864.

[22] Anwer R, Ahmad N, Al Qumaizi KI, Al Khamees OA, Al Shaqha WM, Fatma T. Interaction of procarbazine with calf thymus DNA—a biophysical and molecular docking study. J Mol Recognit 2017;30:e2599. https://doi.org/10.1002/JMR.2599.

[23] Silva MM, Nascimento EOO, Silva EF, Araújo JX de, Santos JCC, Figueiredo IM, et al. Interaction between bioactive compound 11a-N-tosyl-5-deoxi-pterocarpan (LQB-223) and Calf thymus DNA: Spectroscopic approach, electrophoresis and theoretical studies. Int J Biol Macromol 2017;96:223–33. https://doi.org/10.1016/J.IJBIOMAC.2016.12.044.

[24] Jabeen E, Janjua NK, Ahmed S, Tahiri I, Kashif M, Javed A. DNA binding interaction studies of flavonoid complexes of Cu(II) and Fe(II) and determination of their chemotherapeutic potential. Inorganica Chim Acta 2019;496:119048. https://doi.org/10.1016/J.ICA.2019.119048.

[25] Geng S, Wu Q, Shi L, Cui F. Spectroscopic study one thiosemicarbazone derivative with ctDNA using ethidium bromide as a fluorescence probe. Int J Biol Macromol 2013;60:288–94. https://doi.org/10.1016/J.IJBIOMAC.2013.06.002.

[26] Yang H, Zeng Q, He Z, Wu D, Li H. Determination of the DNA binding properties of a

novel PARP inhibitor MK-4827 with calf-thymus DNA by molecular simulations and detailed spectroscopic investigations. New J Chem 2019;43:6702–11. https://doi.org/10.1039/C9NJ00667B.

[27] KiranKumar HN, RohitKumar HG, Advirao GM. Synthesis, DNA binding and cytotoxic activity of pyrimido[4',5':4,5]thieno(2,3-b)quinoline with 9-hydroxy-4-(3-diethylaminopropylamino) and 8-methoxy-4-(3-diethylaminopropylamino) substitutions. J Photochem Photobiol B Biol 2018;178:1–9. https://doi.org/10.1016/J.JPHOTOBIOL.2017.10.022.

[28] Zhu P, Zhang G, Ma Y, Zhang Y, Miao H, Wu Y. Study of DNA interactions with bifenthrin by spectroscopic techniques and molecular modeling. Spectrochim Acta Part A Mol Biomol Spectrosc 2013;112:7–14. https://doi.org/10.1016/J.SAA.2013.04.022.

[29] Das A, Mohammed TP, Kumar R, Bhunia S, Sankaralingam M. Carbazole appended trans-dicationic pyridinium porphyrin finds supremacy in DNA binding/photocleavage over a non-carbazolyl analogue. Dalt Trans 2022;51:12453–66. https://doi.org/10.1039/D2DT00555G.

[30] Lu XY, Lou YY, Zhou KL, Jiang SL, Shi JH. Exploring the binding characteristics of febuxostat, an inhibitor of xanthine oxidase with calf thymus DNA: Multi-spectroscopic methodologies and molecular docking. Https://DoiOrg/101080/1525777020222057534 2022;41:605–24. https://doi.org/10.1080/15257770.2022.2057534.

[31] Mussardo P, Corda E, González-Ruiz V, Rajesh J, Girotti S, Martín MA, et al. Study of non-covalent interactions of luotonin A derivatives and the DNA minor groove as a first step in the study of their analytical potential as DNA probes. Anal Bioanal Chem 2011;400:321–7. https://doi.org/10.1007/S00216-010-4640-5/FIGURES/4.

[32] Rozas I, Alkorta I, Elguero J. Behavior of ylides containing N, O, and C atoms as hydrogen bond acceptors. J Am Chem Soc 2000;122:11154–61. https://doi.org/10.1021/JA0017864/SUPPL_FILE/JA0017864_S.PDF.

[33] Shahabadi N, Hadidi S, Ghasemian Z, Taherpour A. Racemic R,S-venlafaxine hydrochloride–DNA interaction: Experimental and computational evidence. Spectrochim Acta Part A Mol Biomol Spectrosc 2015;145:540–52. https://doi.org/10.1016/J.SAA.2015.03.073.

[34] Arif H, Sohail A, Farhan M, Rehman AA, Ahmad A, Hadi SM. Flavonoids-induced redox cycling of copper ions leads to generation of reactive oxygen species: A potential role in cancer chemoprevention. Int J Biol Macromol 2018;106:569–78. https://doi.org/10.1016/j.ijbiomac.2017.08.049.

[35] Magdy G, Shaldam MA, Belal F, Elmansi H. Multi-spectroscopic, thermodynamic, and molecular docking/dynamic approaches for characterization of the binding interaction between calf thymus DNA and palbociclib. Sci Reports 2022 121 2022;12:1–13. https://doi.org/10.1038/s41598-022-19015-9.

[36] Lyles MB, Cameron IL. Interactions of the DNA intercalator acridine orange, with itself, with caffeine, and with double stranded DNA. Biophys Chem 2002;96:53–76. https://doi.org/10.1016/S0301-4622(02)00036-4.

[37] Ahmad A, Ahmad M. Deciphering the mechanism of interaction of edifenphos with calf thymus DNA. Spectrochim Acta Part A Mol Biomol Spectrosc 2018;188:244–51. https://doi.org/10.1016/J.SAA.2017.07.014.

[38] Li X, Yuan Y, Wang Y, Zhang F, Zhao R, Shao D, et al. Binding study of florfenicol with DNA by multi-spectroscopy and molecular docking techniques. Process Biochem 2021;108:26–33. https://doi.org/10.1016/J.PROCBIO.2021.05.023.

[39] Roudini L, NayebZadeh Eidgahi N, Rahimi HR, Saberi MR, Amiri Tehranizadeh Z, Beigoli S, et al. Determining the interaction behavior of calf thymus DNA with berberine hydrochloride in the presence of linker histone: a biophysical study. Https://DoiOrg/101080/0739110220191574240 2019;38:364–81. https://doi.org/10.1080/07391102.2019.1574240.

[40] Anastassopoulou J. Metal–DNA interactions. J Mol Struct 2003;651–653:19–26. https://doi.org/10.1016/S0022-2860(02)00625-7.

[41] Ottová P, Espinoza-Herrera SJ, Štěpánek J. Magnesium effect on premelting transitions in nucleic acids: DNA duplex and RNA hairpin models. J Mol Struct 2011;993:324–7. https://doi.org/10.1016/J.MOLSTRUC.2010.12.025.

[42] Shamsi MH, Kraatz HB. Interactions of Metal Ions with DNA and Some Applications. J Inorg Organomet Polym Mater 2013;23:4–23. https://doi.org/10.1007/S10904-012-9694-8/FIGURES/7.

[43] Suaifan GARY, Mohammed AAM, Alkhawaja BA. Fluoroquinolones’ Biological Activities against Laboratory Microbes and Cancer Cell Lines. Mol 2022, Vol 27, Page 1658 2022;27:1658. https://doi.org/10.3390/MOLECULES27051658.

[44] Shen LL, Pernet AG. Mechanism of inhibition of DNA gyrase by analogues of nalidixic acid: the target of the drugs is DNA. Proc Natl Acad Sci 1985;82:307–11. https://doi.org/10.1073/PNAS.82.2.307.

[45] Lee HM, Kim JK, Kim SK, Sarma RH. Molecular Modeling Study of the Norfloxacin-DNA Complex. Http://DxDoiOrg/101080/07391102200210506811 2012;19:1083–91. https://doi.org/10.1080/07391102.2002.10506811.

[46] Loredana Elena V, Elena VÎJAN L, Giosanu D. Binding of norfloxacin, enoxacin and enrofloxacin to calf thymus DNA. Rev Roum Chim 2012;57:823–7.

[47] Zhang XX, Brantley SL, Corcelli SA, Tokmakoff A. DNA minor-groove binder Hoechst 33258 destabilizes base-pairing adjacent to its binding site. Commun Biol 2020 31 2020;3:1–9. https://doi.org/10.1038/s42003-020-01241-4.

[48] Healy EF. Quantitative determination of DNA-ligand binding using fluorescence spectroscopy. An undergraduate biochemistry experiment. J Chem Educ 2007;84:1304–7. https://doi.org/10.1021/ED084P1304/SUPPL_FILE/JCE2007P1304W.ZIP.

[49] Zimmer C, Wähnert U. Nonintercalating DNA-binding ligands: Specificity of the interaction and their use as tools in biophysical, biochemical and biological investigations of the genetic material. Prog Biophys Mol Biol 1986;47:31–112. https://doi.org/10.1016/0079-6107(86)90005-2.

[50] Kenđel A, Zavidić V, Miljanić S. Hoechst 33258 aggregation and binding to DNA studied by surface-enhanced Raman spectroscopy. J Raman Spectrosc 2022;53:880–9. https://doi.org/10.1002/JRS.6319.

[51] Vardevanyan PO, Parsadanyan MA, Antonyan AP, Shahinyan MA. Study of complexes of Hoechst 33258 with poly(rA)-poly(rU) depending on various ionic strengths in the water-saline solution. Https://DoiOrg/101080/0739110220201823883 2020;40:1182–8. https://doi.org/10.1080/07391102.2020.1823883.

[52] Wang Y, Schellenberg H, Walhorn V, Toensing K, Anselmetti D. Binding Mechanism of Fluorescent Dyes to DNA Characterized by Magnetic Tweezers. Mater Today Proc 2017;4:S218–25. https://doi.org/10.1016/J.MATPR.2017.09.190.

[53] Jantaree P, Lirdprapamongkol K, Kaewsri W, Thongsornkleeb C, Choowongkomon K, Atjanasuppat K, et al. Homodimers of Vanillin and Apocynin Decrease the Metastatic Potential of Human Cancer Cells by Inhibiting the FAK/PI3K/Akt Signaling Pathway. J Agric Food Chem 2017;65:2299–306. https://doi.org/10.1021/acs.jafc.6b05697.

[54] Venturini D, De Souza AR, Caracelli I, Morgon NH, Da Silva-Filho LC, Ximenes VF. Induction of axial chirality in divanillin by interaction with bovine serum albumin. PLoS One 2017;12. https://doi.org/10.1371/journal.pone.0178597.

[55] Xia K, Zhang G, Li S, Gong D. Groove Binding of Vanillin and Ethyl Vanillin to Calf Thymus DNA. J Fluoresc 2017;27:1815–28. https://doi.org/10.1007/S10895-017-2119-X/FIGURES/11.

[56] Lucas S. The Pharmacology of Indomethacin. Headache J Head Face Pain 2016;56:436–46. https://doi.org/10.1111/HEAD.12769.

[57] Chakraborty R, Bhattacharje G, Baral J, Manna B, Mullick J, Mathapati BS, et al. In-silico screening and in-vitro assay show the antiviral effect of Indomethacin against SARS-CoV-2. Comput Biol Med 2022;147. https://doi.org/10.1016/J.COMPBIOMED.2022.105788.

[58] Husain MA, Ishqi HM, Sarwar T, Rehman SU, Tabish M. Interaction of indomethacin with calf thymus DNA: a multi-spectroscopic, thermodynamic and molecular modelling approach. Medchemcomm 2017;8:1283–96. https://doi.org/10.1039/C7MD00094D.

[59] Lui B, Wee B, Lai J, Khattak Z, Kwok A, Donarelli C, et al. A ten-year review of the impact of the transition from warfarin to direct oral anticoagulant - Has venous thromboembolism treatment become safer? Thromb Res 2022;219:112–20. https://doi.org/10.1016/J.THROMRES.2022.09.006.

[60] Sarwar T, Rehman SU, Husain MA, Ishqi HM, Tabish M. Interaction of coumarin with calf thymus DNA: Deciphering the mode of binding by in vitro studies. Int J Biol Macromol 2015;73:9–16. https://doi.org/10.1016/J.IJBIOMAC.2014.10.017.